

Illumination correction by dehazing for retinal vessel segmentation

Benedetta Savelli*, Alessandro Bria[†], Adrian Galdran[‡], Claudio Marrocco*, Mario Molinara*,
Aurélio Campilho^{‡§}, Francesco Tortorella*

**Department of Electrical and Information Engineering, University of Cassino and Southern Latium, Cassino, Italy*
Email: {b.savelli, c.marrocco, m.molinara, tortorella}@unicas.it

[†]*Department of Molecular Medicine, University La Sapienza of Rome, Italy*
Email: a.bria@{uniroma1.it,unicas.it}

[‡]*INESC TEC, Institute for Systems and Computer Engineering, Technology and Science, Porto, Portugal*
Email: adrian.galdran@inesctec.pt

[§]*Faculdade de Engenharia, Universidade do Porto, Portugal*
Email: campilho@fe.up.pt

Abstract—Assessment of retinal vessels is fundamental for the diagnosis of many disorders such as heart diseases, diabetes and hypertension. The imaging of retina using advanced fundus camera has become a standard in computer-assisted diagnosis of ophthalmic disorders. Modern cameras produce high quality color digital images, but during the acquisition process the light reflected by the retinal surface generates a luminosity and contrast variation. Irregular illumination can introduce severe distortions in the resulting images, decreasing the visibility of anatomical structures and consequently demoting the performance of the automated segmentation of these structures.

In this paper, a novel approach for illumination correction of color fundus images is proposed and applied as preprocessing step for retinal vessel segmentation. Our method builds on the connection between two different phenomena, shadows and haze, and works by removing the haze from the image in the inverted intensity domain. This is shown to be equivalent to correct the nonuniform illumination in the original intensity domain. We tested the proposed method as preprocessing stage of two vessel segmentation methods, one unsupervised based on mathematical morphology, and one supervised based on deep learning Convolutional Neural Networks (CNN). Experiments were performed on the publicly available retinal image database DRIVE. Statistically significantly better vessel segmentation performance was achieved in both test cases when illumination correction was applied.

Keywords-retina; vessel segmentation; illumination correction; dehazing.

I. INTRODUCTION

Retinal photography requires the use of a fundus camera, which is a specialized low power microscope with an attached camera capable of simultaneously illuminating and imaging the retina. It is designed to image the interior surface of the eye, which includes the retina, optic disc, macula, and posterior pole [1]. Retinal fundus images are widely used for diagnosis, screening and treatment of cardiovascular and ophthalmologic diseases [2], including age-related macular degeneration and diabetic retinopathy that are considered two leading causes of blindness in the industrialized countries [3]. These diseases are also known to affect the appearance of the blood vessels in the

retina. Morphological attributes such as length, width, and branching angles can be extracted from the vascular tree to detect the presence and the severity of these disorders [4]. However, manual segmentation of retinal blood vessels is a long and tedious task which requires extensive training and skill. Automatic segmentation of retinal vessels is highly desirable in Computer-Aided Diagnosis systems for large-scale screening of ophthalmic disorders [5]. Recent years have witnessed the rapid development of methods for retinal vessel segmentation, as evidenced by extensive reviews [6]. Supervised methods use labeled data to train a classifier that discriminates between vessel and non-vessel pixels. For example, K-Nearest Neighbors [7], Support Vector Machine [8], AdaBoost [9], and deep learning Convolutional Neural Networks (CNN) [10]. Unsupervised methods use filter responses [11], mathematical morphology [12] or other model-based techniques [13].

Among the problems faced by all these methods, there is nonuniform image illumination resulting from image acquisition. The incident light is shone in through the pupil as the image is acquired, and the spherical geometry of the eye creates significant interreflection and shading artifacts [14]. Correction of these illumination inhomogeneities is highly desirable for obtaining high quality results of retinal blood vessel segmentation. Several techniques have been proposed over the years to improve uneven illumination and contrast levels in retinal fundus images. For instance, methods that estimate the illumination profile using B-spline based models [15] or Laplace interpolation [16], and methods that work in the frequency domain with filtering approaches [17] or gradient distribution analysis [18]. The interested reader can refer to Rasta et al. [19] for a recent and more comprehensive review of this field.

In this work, we propose a novel method that builds on the connection between shadows and haze, an apparently unrelated phenomenon that causes image degradation due to atmospheric absorption and scattering. We show that removing the haze from the image in the inverted intensity

domain is equivalent to correct the nonuniform illumination in the original intensity domain. We implemented and tested two different vessel segmentation methods to verify the effectiveness of the proposed method as preprocessing stage. The first is an unsupervised method based on a sequence of denoising and morphological filters, whereas the second is a supervised method based on a customized deep learning Convolutional Neural Network (CNN).

II. ILLUMINATION CORRECTION BY DEHAZING

The problem of illumination correction consists of solving the illumination-reflectance model of image formation described by the following multiplicative relationship:

$$I(x) = i(x)r(x) \quad (1)$$

where $I(x)$ is the captured image intensity (graylevel or RGB) corresponding to the pixel x , $i(x)$ describes the illumination conditions affecting the scene, and $r(x)$ is the true reflectance of the object that we want to estimate. Assuming image intensities normalized in $[0, 1]$, we can solve this problem in the inverted intensity domain $1 - I(x)$ so that Eq. 1 rewrites as:

$$1 - I(x) = 1 - i(x)r(x) \quad (2)$$

which by simple algebraic manipulations can be written as:

$$1 - I(x) = (1 - r(x))i(x) + 1 - i(x) \quad (3)$$

Let us now denote with $\tilde{I}(x) = 1 - I(x)$ and $\tilde{r}(x) = 1 - r(x)$ the captured intensity and true reflectance in the inverted intensity domain, respectively. Then, Eq. 3 rewrites as:

$$\tilde{I}(x) = i(x)\tilde{r}(x) + 1 - i(x) \quad (4)$$

which is closely related to the problem of haze degradation modeled by the following image formation law [20]:

$$I(x) = t(x)R(x) + A - At(x) \quad (5)$$

where $R(x)$ is the radiance in a hypothetical haze-free scene, $t(x)$ is the transmission of light in the atmosphere, and A is the predominant color of the atmosphere. Following [21], we can assume that the input image has been white-balanced, so that the greatest intensity in the image is white and A can be approximated by $A \approx (1, 1, 1)$. Then, the haze degradation model simplifies in:

$$I(x) = t(x)R(x) + 1 - t(x) \quad (6)$$

which is the dual formulation of Eq. 4 that can be obtained by exchanging $r(x)$ with $R(x)$ (reflectance with radiance) and $i(x)$ with $t(x)$ (illumination with transmission).

The dualism between dehazing and illumination correction is supported by the key observation that haze and shadows share a common feature: both are low-frequency, slowly varying phenomena. The presence of haze drives true colors towards white, whereas shadows drive them towards

darker intensities. According to this, we can reformulate the illumination correction problem as follows:

- 1) given an image $I(x)$ affected by the presence of shadows, invert its intensities $\tilde{I}(x) = 1 - I(x)$
- 2) in the inverted intensity domain $\tilde{I}(x)$, solve the problem of haze removal by estimating $t(x)$ and factoring the true radiance $R(x)$
- 3) invert the intensities of $R(x)$ to get the illumination corrected image

To estimate $t(x)$, we apply the popular Dark-Channel prior method [22]. It is based on the observation that most local patches in haze-free images contain some pixels which have very low intensity in at least one color channel (the so-called dark channel). Using this prior with the haze imaging model, it is possible to directly estimate $t(x)$ as:

$$t(x) \approx 1 - \omega \frac{\tilde{I}_{\text{dark}}(x)}{A} \quad (7)$$

where ω is a constant parameter, and $\tilde{I}_{\text{dark}}(x)$ is the dark channel of the inverted image $\tilde{I}(x)$ estimated in a local neighborhood $\Omega(x)$ as:

$$\tilde{I}_{\text{dark}}(x) = \min_{c \in \{R, G, B\}} \left(\min_{z \in \Omega(x)} \tilde{I}(z) \right) \quad (8)$$

The result of applying this technique with $\omega = 0.9$ and a neighborhood of side $d = 20$ pixels is shown in Fig. 1.

III. DATASET

The proposed approach for illumination correction was applied to the images of the Digital Retinal Images for Vessel Evaluation (DRIVE) publicly available database [23]. This dataset has been established to enable comparative studies on segmentation of blood vessels in retinal images. The photographs for the DRIVE database were obtained from a diabetic retinopathy screening program in The Netherlands. The images were acquired using a Canon CR5 non-mydratric 3CCD camera with a 45 degree field of view (FOV). Each image was captured using 8 bits per color plane and consisted of 768×584 pixels. The dataset consisted of 40 images equally distributed in a training and test set. We applied our illumination correction on both training and test sets with parameters $\omega = 0.9$, and $d = 20$ chosen in relation to the vessel width. These parameters were fixed at the beginning of our experiments and were not varied afterwards.

IV. RETINAL VESSEL SEGMENTATION

A. Unsupervised

The unsupervised retinal vessel segmentation that we implemented consists of three steps: (i) green channel extraction; (ii) denoising; and (iii) vessel enhancement by means of grayscale mathematical morphology. These steps are detailed as follows. First, the green channel is extracted from the RGB image since it provides better vessel-to-background



Figure 1. (a) A retinal image suffering from the presence of nonuniform illumination, and (b) the result of the illumination correction by dehazing.

contrast compared to the other two channels. Then, non-local means denoising [24] is applied. This algorithm reduces the noise while preserving the characteristics of the vessel intensity profiles. A vessel is characterized by a dark pattern with Gaussian-shape cross-section profile, piecewise connected, and locally linear. This key observation allows us to enhance vessels with a series of morphological top-hat transforms, each targeting a specific vessel orientation. Given the input image f , the black top-hat transform (BTH) is defined as the difference between the closing of f and f :

$$\text{BTH}(f, b) = f \bullet b - f \quad (9)$$

where $f \bullet b$ denotes the closing of f by the structuring element (SE) b . This operation enhances the objects that are smaller than b (i.e., in which b does not fit) and darker than their surroundings. In this context, b is chosen as a linear SE b_L slightly longer than the width L of primary (large) vessels. In this way, all the vessels orthogonal to b_L will be enhanced by $\text{BTH}(f, b_L)$. Applying multiple $\text{BTH}(f, b_L^\theta)$ for N different angles θ equally spaced in $[0, \pi)$ will enhance different portions of the vessel tree. The sum of top-hats (STH) yields the enhancement of the entire vessel tree:

$$\text{STH}(f, b_L) = \sum_{\theta} (f \bullet b_L^\theta - f) \quad (10)$$

which can be thresholded to generate the vessel tree segmentation according to the desired sensitivity/specificity level. The length L of b_L and the number N of angles were chosen as $L = 16$ and $N = 12$ based on the visual inspection of the images and on the segmentation accuracy achieved on the training set. Of note, the performances did not vary significantly in the parameter range $L \in [12, 20]$ and $N \in [10, 16]$, suggesting that this approach is robust with respect to the choice of its parameters.

B. Supervised method

We used a supervised approach for retinal vessel segmentation based on CNN. A CNN is an ensemble of units, each involving several weighted inputs and one output, performing convolution of inputs with weights and transforming the outcome according to a nonlinear activation function. Units are arranged in layers and usually share the same weights so as to produce a feature map and reduce the number of parameters. In a typical CNN architecture, convolutional layers interlaced with max-pooling layers that aggregate the outputs of multiple units and return the maximum. The final decision is made through one or more fully connected layers that consider all the outputs of the units of the previous layer.

In this paper, we used a CNN inspired by the work of Liskowski and Krawiec [10] that recently obtained the state-of-the-art performance in the automated retinal vessel segmentation. To train the network, image patches of dimensions 27×27 were extracted from the green channel of the 20 images of the training set. Each patch was associated to a binary class label (vessel or background) according to the class of the central pixel of the patch. Only patches that completely fit in the field of view were considered. For the training phase we randomly sampled 800,000 patches, equally divided into vessels and background, whereas for the test phase all the patches extracted from each test image were considered. The network architecture is reported in Table I together with the parameters of each layer. All the convolutional layers were equipped with the Rectified Linear Units (ReLU) that apply a nonsaturating activation function ($f(x) = \max(0, x)$). Two dropout layers were also used after the first two fully connected layers to reduce overfitting. The dropout was performed with a probability of 0.5 indicating that, at each training stage, half of the

Table I
ARCHITECTURE OF THE CNN

Layer	Type	Output size	Kernel Size	Stride	Padding
0	Input	$1 \times 27 \times 27$			
1	Convolutional	$64 \times 26 \times 26$	4×4	1	1
2	ReLU	$64 \times 26 \times 26$			
3	Convolutional	$64 \times 26 \times 26$	3×3	1	1
4	ReLU	$64 \times 26 \times 26$			
5	Max pooling	$64 \times 13 \times 13$	2×2	2	0
6	Convolutional	$128 \times 13 \times 13$	3×3	1	1
7	ReLU	$128 \times 13 \times 13$			
8	Convolutional	$128 \times 13 \times 13$	3×3	1	1
9	ReLU	$128 \times 13 \times 13$			
10	Max pooling	$128 \times 6 \times 6$	2×2	2	0
11	FC	512	1×1		
12	Dropout	512			
13	FC	512	1×1		
14	Dropout	512			
15	FC	2	1×1		

units coming from the previous layer were ignored in the training of the successive layer. Weights in all the layers were initialized using the algorithm of Glorot and Bengio [25]. The network was trained to minimize the Softmax loss function by means of backpropagation and Mini-Batch Stochastic Gradient Descent, with mini-batches of 32 samples. Standardization was applied to the inputs by mean subtraction and normalization to unit variance [26]. The learning rate was initially set to 10^{-3} and decreased by a factor of 10 every 120,000 iterations. In total, the learning rate was decreased 5 times, and the learning was stopped after 24 epochs (1 epoch = 25,000 iterations), i.e., when the loss function did not decrease significantly. Momentum and weight decay were set respectively to 0.9 and 5×10^{-4} . We used the Caffe framework [27] for the implementation of the network, and all the experiments were conducted on a machine with 2 Intel Xeon e5-2609 processors, 256 GB of RAM and 2 GPU NVIDIA TitanX Pascal.

V. RESULTS

The performances of the segmentation algorithms were evaluated on the 20 test images of the DRIVE database, with and without preprocessing. All algorithms produced soft output images in which pixels were associated with a degree of membership to the vessel class. The Receiving Operator Characteristics (ROC) curves were then computed with the True Positive Ratio (TPR) versus the False Positive Ratio (FPR) with respect to the varying threshold value applied to the soft outputs. A close-up of the resulting ROC curves is shown in Fig. 2 for typical sensitivity/specificity

Table II
AUC% AND ACCURACY% PERFORMANCES OF VESSEL SEGMENTATION APPLIED TO THE TEST IMAGES IN DRIVE W/O PREPROCESSING (UNPRO) AND W/ ILLUMINATION CORRECTION BY DEHAZING (DH). STATISTICALLY SIGNIFICANTLY RESULTS ARE LISTED IN BOLD.

Method	Metric	UNPRO	DH	DH – UNPRO
Sum of top-hats	AUC	93.79	93.93	+0.14 ($p < 0.001$)
Sum of top-hats	Accuracy	94.40	94.53	+0.13 ($p < 0.001$)
CNN	AUC	97.07	97.29	+0.23 ($p < 0.001$)
CNN	Accuracy	94.76	94.93	+0.17 ($p < 0.001$)

ranges (TPR $\geq 70\%$ and $1 - \text{FPR} \geq 90\%$). To quantify the performance of the different methods, the area under the ROC curve (AUC) was calculated. AUC is a measure suitable even when the samples in the two classes are unbalanced, as is the case of the blood vessels in retinal images, where the number of non-vessel pixels is higher than the number of vessel pixels [28]. In Table II (columns 3-4) AUC performance is reported along with the classification accuracy, which is commonly adopted in the literature.

To determine statistically significant differences in AUC and accuracy, we applied the bootstrap procedure [29] as in [30]. The test set was randomly sampled with replacement 1,000 times so that each new set of sampled data contained the same number of examples as the original set. For each vessel segmentation method, we calculated the differences in AUC and accuracy between the illumination-corrected and unprocessed images. Resampling 1,000 times resulted in 1,000 values for the performance differences. P -values were defined as the fraction of values that were negative or zero, corresponding to cases in which the vessel segmentation with preprocessing performed worse or equally than without preprocessing. The statistical significance level was chosen as 5% and, thus, performance differences were considered statistically significant if $p < 0.05$. The resulting performance differences are reported in Table II (column 5). In all cases, a statistically significantly better performance was achieved when illumination correction was applied.

VI. DISCUSSION AND CONCLUSIONS

In the present study, we have established a new connection between the problem of illumination correction in retinal color fundus images and the apparently unrelated problem of haze removal in open-air images. We applied a popular dehazing method, namely the Dark Channel prior method, to the images in the inverted intensity domain. This resulted in an illumination correction of the original images that enhanced the performance of vessel segmentation. We showed this using two different segmentation approaches, one supervised and one unsupervised, obtaining similar improvements for both methods. Even though statistically significant, the improvement in performance was rather

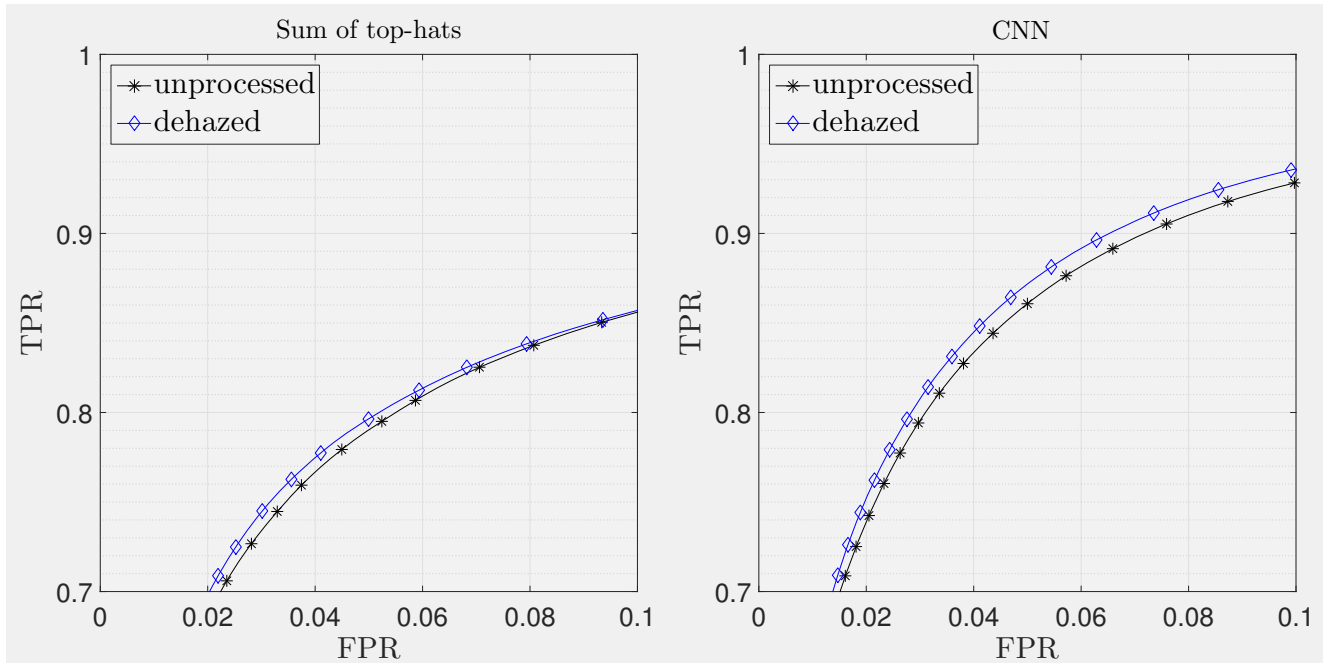


Figure 2. Partial ROC curves of the two vessel tree segmentation algorithms applied to the test images in DRIVE before (unprocessed) and after (dehazed) preprocessing.

small, ranging between +0.14 and +0.23 of AUC%. It should be noted, however, that the DRIVE database contains images selected ad-hoc for the task of automated vessel segmentation. For example, using the DRIIL (Digital Retinal Images for ILLumination correction) database [31], that spans a wide range of illumination conditions, could yield better improvements. However the DRIIL database lacks vessel annotations. In future work we will investigate how to combine DRIVE and DRIIL databases to yield a new set of images suited for both vessel segmentation and illumination correction. Future directions also include experimenting other existing dehazing methods to solve the illumination correction model proposed in this work, and testing these methods in combination with a wide selection of vessel segmentation algorithms and methods designed to face the asymmetry between the classes [32], [33]. If successful, this would lead to an entire new family of simple and effective alternative illumination correction methods.

ACKNOWLEDGMENT

The authors affiliated to the University of Cassino and Southern Latium gratefully acknowledge the support of NVIDIA Corporation for the donation of the Titan X Pascal GPUs used for this research.

A. Galdran and A. Campilho were financed by the ERDF European Regional Development Fund through the Operational Programme for Competitiveness and Internationalisation - COMPETE 2020 Programme, and by National Funds

through the FCT - Fundação para a Ciência e a Tecnologia within project CMUP-ERI/TIC/0028/2014.

REFERENCES

- [1] R. J. Winder, P. J. Morrow, I. N. McRitchie, J. Bailie, and P. M. Hart, "Algorithms for digital image processing in diabetic retinopathy," *Computerized Medical Imaging and Graphics*, vol. 33, no. 8, pp. 608–622, 2009.
- [2] M. M. Fraz, P. Remagnino, A. Hoppe, B. Uyyanonvara, A. R. Rudnicka, C. G. Owen, and S. A. Barman, "Blood vessel segmentation methodologies in retinal images—a survey," *Computer Methods and Programs in Biomedicine*, vol. 108, no. 1, pp. 407–433, 2012.
- [3] M. D. Abràmoff, J. C. Folk, D. P. Han, J. D. Walker, D. F. Williams, S. R. Russell, P. Massin, B. Cochener, P. Gain, L. Tang *et al.*, "Automated analysis of retinal images for detection of referable diabetic retinopathy," *JAMA ophthalmology*, vol. 131, no. 3, pp. 351–357, 2013.
- [4] G. Leontidis, B. Al-Diri, J. Wigdahl, and A. Hunter, "Evaluation of geometric features as biomarkers of diabetic retinopathy for characterizing the retinal vascular changes during the progression of diabetes," in *Engineering in Medicine and Biology Society (EMBC), 2015 37th Annual International Conference of the IEEE*. IEEE, 2015, pp. 5255–5259.
- [5] S. W. Franklin and S. E. Rajan, "Computerized screening of diabetic retinopathy employing blood vessel segmentation in retinal images," *Biocybernetics and Biomedical Engineering*, vol. 34, no. 2, pp. 117–124, 2014.

- [6] N. Singh and L. Kaur, "A survey on blood vessel segmentation methods in retinal images," in *Electronic Design, Computer Networks & Automated Verification (EDCAV), 2015 International Conference on*. IEEE, 2015, pp. 23–28.
- [7] J. Staal, M. D. Abràmoff, M. Niemeijer, M. A. Viergever, and B. Van Ginneken, "Ridge-based vessel segmentation in color images of the retina," *IEEE Transactions on Medical Imaging*, vol. 23, no. 4, pp. 501–509, 2004.
- [8] X. You, Q. Peng, Y. Yuan, Y.-m. Cheung, and J. Lei, "Segmentation of retinal blood vessels using the radial projection and semi-supervised approach," *Pattern Recognition*, vol. 44, no. 10, pp. 2314–2324, 2011.
- [9] C. A. Lupascu, D. Tegolo, and E. Trucco, "Fabc: retinal vessel segmentation using adaboost," *IEEE Transactions on Information Technology in Biomedicine*, vol. 14, no. 5, pp. 1267–1274, 2010.
- [10] P. Liskowski and K. Krawiec, "Segmenting retinal blood vessels with deep neural networks," *IEEE Transactions on Medical Imaging*, vol. 35, no. 11, pp. 2369–2380, 2016.
- [11] G. Azzopardi, N. Strisciuglio, M. Vento, and N. Petkov, "Trainable cosfire filters for vessel delineation with application to retinal images," *Medical Image Analysis*, vol. 19, no. 1, pp. 46–57, 2015.
- [12] G. Hassan, N. El-Bendary, A. E. Hassanien, A. Fahmy, V. Snasel *et al.*, "Retinal blood vessel segmentation approach based on mathematical morphology," *Procedia Computer Science*, vol. 65, pp. 612–622, 2015.
- [13] Y. Zhao, L. Rada, K. Chen, S. P. Harding, and Y. Zheng, "Automated vessel segmentation using infinite perimeter active contour model with hybrid region information with application to retinal images," *IEEE Transactions on Medical Imaging*, vol. 34, no. 9, pp. 1797–1807, 2015.
- [14] M. Foracchia, E. Grisan, and A. Ruggeri, "Luminosity and contrast normalization in retinal images," *Medical Image Analysis*, vol. 9, no. 3, pp. 179–190, 2005.
- [15] L. Kubecka, J. Jan, and R. Kolar, "Retrospective illumination correction of retinal images," *Journal of Biomedical Imaging*, vol. 2010, p. 11, 2010.
- [16] C. Leahy, A. O'Brien, and C. Dainty, "Illumination correction of retinal images using Laplace interpolation," *Applied optics*, vol. 51, no. 35, pp. 8383–8389, 2012.
- [17] W. A. Mustafa, H. Yazid, and S. B. Yaacob, "Illumination correction of retinal images using superimpose low pass and gaussian filtering," in *Biomedical Engineering (ICoBE), 2015 2nd International Conference on*. IEEE, 2015, pp. 1–4.
- [18] Y. Zheng, B. Vanderbeek, R. Xiao, E. Daniel, D. Stambolian, M. Maguire, J. O'Brien, and J. Gee, "Retrospective illumination correction of retinal fundus images from gradient distribution sparsity," in *Biomedical Imaging (ISBI), 2012 9th IEEE International Symposium on*. IEEE, 2012, pp. 972–975.
- [19] S. H. Rasta, M. E. Partovi, H. Seyedarabi, and A. Javadzadeh, "A comparative study on preprocessing techniques in diabetic retinopathy retinal images: Illumination correction and contrast enhancement," *Journal of Medical signals and sensors*, vol. 5, no. 1, p. 40, 2015.
- [20] H. Koschmieder, *Theorie der horizontalen Sichtweite: Kontrast und Sichtweite*. Keim & Nemnich, 1925.
- [21] J.-P. Tarel and N. Hautiere, "Fast visibility restoration from a single color or gray level image," in *Computer Vision, 2009 IEEE 12th International Conference on*. IEEE, 2009, pp. 2201–2208.
- [22] K. He, J. Sun, and X. Tang, "Single Image Haze Removal Using Dark Channel Prior," *IEEE Transactions on Pattern Analysis and Machine Intelligence*, vol. 33, no. 12, pp. 2341–2353, 2011.
- [23] J. Staal, M. D. Abràmoff, M. Niemeijer, M. A. Viergever, and B. Van Ginneken, "Ridge-based vessel segmentation in color images of the retina," *IEEE Transactions on Medical Imaging*, vol. 23, no. 4, pp. 501–509, 2004.
- [24] A. Buades, B. Coll, and J.-M. Morel, "Non-local means denoising," *Image Processing On Line*, vol. 1, pp. 208–212, 2011.
- [25] X. Glorot and Y. Bengio, "Understanding the difficulty of training deep feedforward neural networks." in *Aistats*, vol. 9, 2010, pp. 249–256.
- [26] Y. A. LeCun, L. Bottou, G. B. Orr, and K.-R. Müller, "Efficient backprop," in *Neural networks: Tricks of the trade*. Springer, 2012, pp. 9–48.
- [27] Y. Jia, E. Shelhamer, J. Donahue, S. Karayev, J. Long, R. Girshick, S. Guadarrama, and T. Darrell, "Caffe: Convolutional architecture for fast feature embedding," *arXiv preprint arXiv:1408.5093*, 2014.
- [28] W. S. Oliveira, J. V. Teixeira, T. I. Ren, G. D. Cavalcanti, and J. Sijbers, "Unsupervised retinal vessel segmentation using combined filters," *PloS one*, vol. 11, no. 2, p. e0149943, 2016.
- [29] F. W. Samuelson and N. Petrick, "Comparing image detection algorithms using resampling," in *IEEE Int. Symp. Biomed. Imag.*, 2006, pp. 1312–1315.
- [30] A. Bria, C. Marrocco, M. Molinara, and F. Tortorella, "An effective learning strategy for cascaded object detection," *Information Sciences*, vol. 340, pp. 17–26, 2016.
- [31] R. Kolar, J. Odstrcilik, J. Jan, and V. Harabis, "Illumination correction and contrast equalization in colour fundus images," in *Signal Processing Conference, 2011 19th European*. IEEE, 2011, pp. 298–302.
- [32] A. Bria, C. Marrocco, M. Molinara, and F. Tortorella, "A ranking-based cascade approach for unbalanced data," in *Pattern Recognition (ICPR), 2012 21st International Conference on*. IEEE, 2012, pp. 3439–3442.
- [33] G. Haixiang, L. Yijing, J. Shang, G. Mingyun, H. Yuanyue, and G. Bing, "Learning from class-imbalanced data: Review of methods and applications," *Expert Systems with Applications*, 2016.